JOURNAL OF AIRCRAFT
Vol. 47, No. 5, September–October 2010

Engineering Notes

Experimental Investigation into Articulated Winglet Effects on Flying Wing Surface Pressure Aerodynamics

A. Gatto*
Brunel University,
Uxbridge, England UB8 3PH, United Kingdom
P. Bourdin†
Bombardier Aerospace, Toronto, Ontario M3K 1Y5, Canada
and
M. I. Friswell‡
University of Swansea,
Swansea, Wales SA2 8PP, United Kingdom

DOI: 10.2514/1.C000251

Nomenclature

C_p = pressure coefficient
y = spanwise station from wing root, mm
α = angle of attack, deg
Γ = dihedral angle of the winglet measured relative to wing plane, deg
Δ = change or difference

I. Introduction

FOR the majority of the last century, the primary means for aircraft control through the use of elevators for pitch control, ailerons for roll control, and a rudder for yaw control has remained largely unchallenged. For aircraft designers around the world, this control methodology represents the most reliable, robust, generally applicable, and effective means of aircraft attitude control that currently exists. While it is certainly true that this method of aircraft control has become much more complex as the rapid advance in aerospace technologies continues to accelerate [1], a wide-ranging successor to this traditional method that can significantly improve upon this baseline method, giving substantial improvements in efficiency and performance, continues to remain operationally complex and/or difficult to justify.

While this required and necessary search remains ongoing, the use of this traditional method of aircraft control does rely on the deflection of hinged, discrete control surfaces, which can, even under moderate levels of deflection, set up localized areas of severe adverse pressure gradients (typically along the hinge line) that both promote and produce regions of flow separation. Under these conditions, both control surface and overall wing efficiency are reduced, leading to suboptimal aircraft performance. This drawback of the current system is one of the main reasons the search for "morphing" aircraft systems and technologies continues [2–9]. If successful, and through using control configurations that allow more general and subtle changes in streamwise curvature, morphing for control may lead to increases in aerodynamic efficiency while maintaining comparable performance.

In this Note, work is presented that extends a concept for a novel aircraft roll control system considered in an earlier paper by the authors [10]. The focus of this Note will principally consider the influence of articulated winglets on the resulting surface pressures on a flying wing test model for possible applications to gust load alleviation. The experimental model tested, analyzed, and evaluated used two actively controlled wingtips (one mounted at each wingtip) that were free to rotate about the wingtip chord axis line. The model was also purposely built to allow for multiple dynamic surface pressure measurements on one upper wing surface to measure, under test conditions, the real-time aerodynamic changes during winglet actuation.

II. Experimental Setup and Apparatus

A. Flying Wing Model

A schematic of the swept wing model designed and built for the test program is shown in Fig. 1. The baseline configuration (without winglets) used a Zagi 12 wing section, a 30 deg leading-edge sweep, a wingspan of 1.2 m (1.54 m with winglets planar), zero washout, and root and tip chords of 0.326 and 0.185 m, respectively. All sections of the complete wing (comprising the main baseline wing sections and the winglets) were made of a blue foam core that was reinforced and strengthened with a bonded carbon and lacquered skin to further resist aerodynamic loading and produce an aerodynamically robust surface finish. To build the flying wing configuration, the two mirrored baseline semispan wing sections were mated and glued together at the root, using additional carbon stiffening rods for extra strength. Before assembly, and to allow for the integration of the active wingtip actuator assembly and the array of dynamic pressure transducers, sections of the undersurface of each baseline wing semispan section at the wing tip were removed. Internal portions of the blue foam core within the starboard (looking from behind the model) baseline semispan wing and winglet were also removed to accommodate integration of the dynamic surface pressure transducer array.

Fifty-seven Honeywell CPC 1 psi dynamic pressure sensors with identical custom-built amplifier electronics were used to measure the dynamic surface pressures on both the starboard baseline semiwing span and the winglet combination. All pressure sensors used to instrument the model had a spatial footprint of less than $20 \times 10 \times 5$ mm^3 (including customized electronics), which allowed for the integration of the pressure sensors in regions of interest close to the wing/winglet juncture as well as near the trailing edge of both the baseline wing and the winglet. The chosen placement of the pressure transducers is shown in Fig. 2. Initially, each pressure transducer was fixed in these positions with the exposed portion of the main active pressure port protruding out of the upper wing surface, exposing it to the main wing surface flow. To ensure that there was no undue aerodynamic contamination, each of these exposed sections were trimmed and sanded back to the main wing surface, creating an aerodynamically smooth surface finish. Signal lines from all installed pressure transducers were channeled through the main wing section, exiting at the root spanwise station, and down the purposely designed and built wind-tunnel support sting. For the active winglet, the control lines for the installed pressure transducers were carefully channeled through the wing/winglet interface support (Fig. 1), taking particular consideration to ensure that the winglet maintained a free and unhindered ability to rotate about its axis. This interface support

Received 13 January 2010; revision received 26 March 2010; accepted for publication 8 May 2010.

*Lecturer in Aerospace Engineering, Department of Mechanical Engineering. Senior Member AIAA.
†Engineering Analyst, Core Engineering.
‡Professor, School of Engineering.

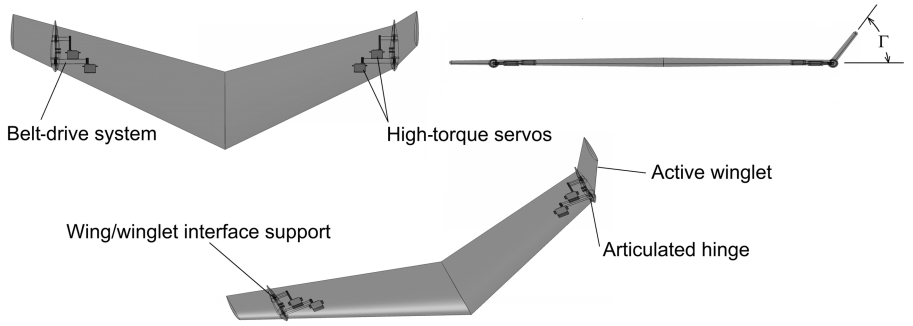

Fig. 1 General schematic of the baseline flying wing with active winglets.

(body of revolution) was manufactured and installed to facilitate seamless and aerodynamically efficient rotation of the winglet around the baseline wing plane. All data obtained were digitized through the 16-bit dSpace data acquisition and control system, at 1000 Hz, over a period of 30–60 s, depending on the test configuration.

Together with the surface pressure transducers, seven dynamic pressure sensors identical to those used to obtain wing surface information were also installed at strategic locations throughout the starboard wing and winglet internal cavities (internal pressure sensor locations also indicated in Fig. 2) to measure the internal cavity pressures during test conditions. Installation of these internal sensors, together with the surface pressure transducers, was carefully controlled and managed with all exposed main access wing/winglet covers and gaps surrounding the sensors sealed from exposure to the outside flowfield. One active port of all these installed internal pressure sensors was connected to a single pneumatic plastic tube (via several offshoot branches), allowing a common reference for measurement and/or correction of internal static pressures offsets, if necessary, in the surface pressure results obtained. The other end of this tube, which was fed out of the model (at the wing root) and test section of the wing tunnel, was left exposed to static atmospheric conditions within the laboratory environment. As the internal cavity static pressures within the model were found to not vary significantly during tests, no corrections for the lag effects of the tubing were applied. Before test program initiation, initial testing of the pressure sensor/amplifier combination resulted in a measured combined nonlinearity and hysteresis of $\pm 2\%$ (full-scale deflection) and a linear frequency response up to 500 Hz. Additionally, the calibration of each pressure sensor was checked in situ against a Digitron 2081P pressure meter and found to lie within a 95% confidence interval of $\pm 3\%$ (full-scale deflection).

To achieve winglet rotation, two digital Hitec HSR-5995TG robot servos, located at each wing tip, were built into the baseline wingtip assembly. Both sets of servos were retrofitted with a belt-drive system operating with a 1:1 gear ratio to rotate the winglets through a connected shaft within the wing/winglet interface support (Fig. 1). The actuation torque produced by the servos was transferred from this shaft to the articulated winglet through four mounting struts that were all screwed and glued to a support frame within the active winglet. To ensure that both servos for each active winglet worked in unison, the signal lines from each servo were connected together, allowing a single control signal to operate both servos.

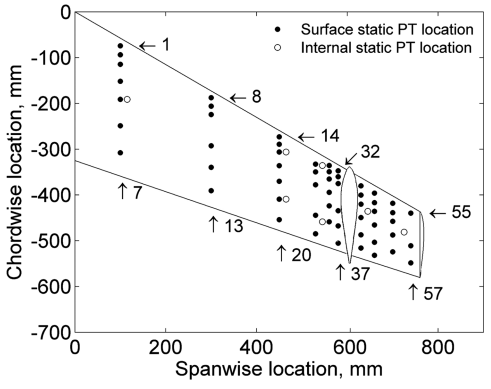

Fig. 2 Position of surface and internal pressure transducer locations within the wing/winglet model (PT denotes pressure transducer).

B. Wind-Tunnel Measurement Environment

The experimental setup for the baseline swept wing/winglet combination is shown in Fig. 3. The model was installed at midtest-section height using a specifically designed support strut inside a closed test section (height = 1.5 m and width = 2.1 m), and a closed circuit wind tunnel with a maximum operating freestream velocity of 60 ± 1 ms^{-1}. The nominal flow speed under test conditions was selected at 30 ms^{-1}, giving a Reynolds number based on the mean aerodynamic chord of the baseline configuration of 5.53×10^5. At the model station, the freestream turbulence level was approximately 0.2%. No wind-tunnel blockage corrections or artificial transition fixing on the model were applied throughout the entire test program.

All four servos used to control and actuate the winglet were driven by a dSpace control system. This system was configured to generate pulse width modulated input signals, at 50 Hz, with variable duty cycles corresponding to a pulse width range of between 400–2100 μs. The calibration of winglet dihedral angular position was carried out using a digital inclinometer (error $\pm 0.1\%$) positioned on the control surfaces and matched to a readout from the dSpace control system indicating the input signal pulse width. Under wind-on conditions, the demanded input was found to be achieved within an error range of $\pm 4^\circ$ with a maximum achievable dihedral angle deflection for the active winglets being ± 75 deg (positive dihedral-winglet rotation above the wing plane). The same digital inclinometer was used to calibrate the angle of attack of the model that was fixed within the range of 0–12 deg (position error ± 1 deg) in increments of 4 deg.

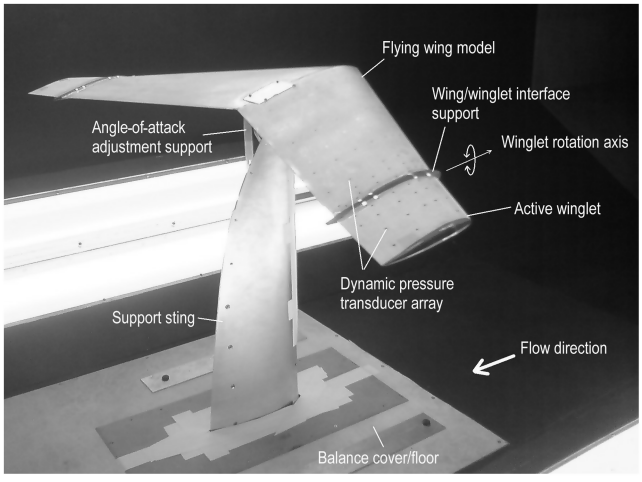

Fig. 3 Experimental setup for active wingtip flying wing.

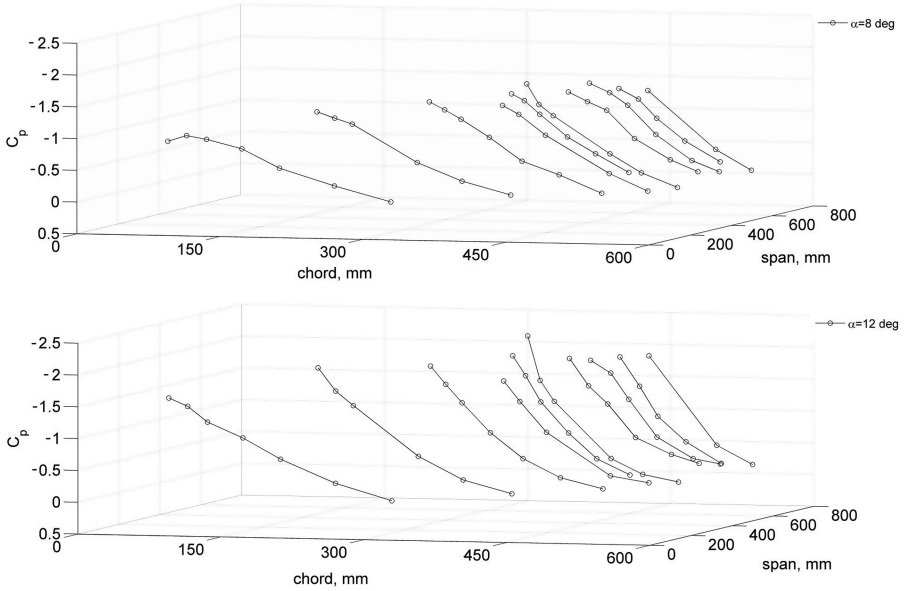

Fig. 4 Wing/winglet surface pressures with $\Gamma = 0$ deg and $Re_n = 5.53 \times 10^5$.

III. Results and Discussion

An example of the mean surface pressures measured on the upper surface of the starboard wing/winglet combination is shown in Fig. 4. On first inspection, the baseline C_p results at both angles of attack show successive minimum peaks toward the leading edge of the model, reducing to near $C_p = 0$ as the chordwise position reaches the trailing edge of the wing. At stations 20, 25, and 37, which were located in close proximity to the trailing edge, surface pressures indicated small positive values, indicating the influence of the reflex trailing-edge profile used on the surface pressures. At the spanwise station most inboard for $\alpha = 8$ deg, the peak in the minimum pressure was found to occur at station 2 with $C_p = -0.998$ moving to $C_p = -1.313$ at station 14 to the maximum negative pressure measured (station 32) of $C_p = -1.519$. This level of negative pressure coefficient was generally maintained on the winglet itself as well ($C_p = -1.362$: station 38, $C_p = -1.374$: station 50), which would be expected as the chosen wing configuration was untwisted (wingtip more heavily loaded). At station 32, located just before the

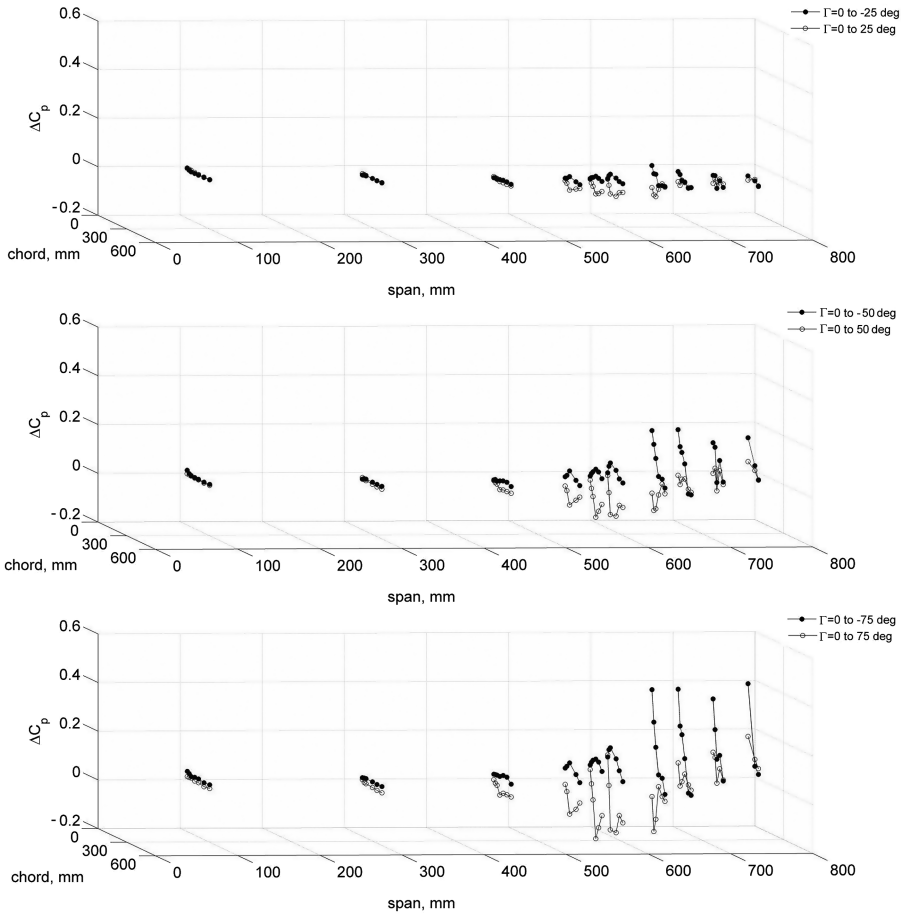

Fig. 5 Change in wing/winglet surface pressures for $\alpha = 8$ deg and $Re_n = 5.53 \times 10^5$.

wing/winglet interface juncture toward the leading edge, the magnitude of the peak was found to be more than 11% higher than that found from the nearest neighbor (station 26 with $C_p = -1.311$), suggesting the existence of a local area of flow acceleration resulting most probably from interaction between the oncoming flow and the inboard leading-edge face of the interface support at $y = 600$ mm. This area of increased suction at these spanwise and chordwise locations was also found for the case of $\alpha = 12$ deg.

The influence of actively rotating the winglet both above and below the wing plane though various levels of dihedral is presented in Figs. 5 and 6. For clarity of presentation, the results measured on the winglet are presented without the relevant position change out of the wing plane, which occurred in reality from winglet rotation. For small deflections in dihedral, the influence on both the wing and winglet surface pressure distributions were only moderate. Under these conditions, the variation in the three most inboard spanwise stations (closest to the wing root) is almost negligible, with a maximum change to the C_p distribution being less than $\pm 4\%$ (located at station 19). However the influence of winglet deflection, even at these very small levels of winglet deflection of $\Gamma = \pm 25$ deg, begins to show a significant level of influence on the surface pressure distribution at the three spanwise measurement planes just inboard of the wing/winglet interface support. Within this localized wing area, both deflections above and below the wing plane have a measurable influence on the pressure distribution, the maximum deviations from the mean C_p values being larger for winglet deflection above the wing plane ($\Delta C_p = -0.0487$ or -4.9% at station 34 for Γ between 0 and 25 deg) than those measured below the wing plane ($\Delta C_p = 0.0325$ or 3.2% at station 34 for Γ between 0 and -25 deg), as the winglet confines and helps to maintain negative upper surface pressure magnitudes.

Considering more extreme winglet dihedral deflections for the ± 50 deg and ± 75 deg cases, also shown in Fig. 5, larger winglet deflections have both more significant and more disruptive effects, not only for spanwise stations close to the interface support juncture but also at further inboard stations. This influence for winglet deflections of $\Gamma = \pm 75$ deg is shown to extend, with significant effects, out to now four spanwise locations inboard of the wing/winglet interface support ($450 \leq y \leq 600$ mm) with minor, but detectable, changes evident for the remaining spanwise measurement locations on the main wing ($y = 100$ and 300 mm). The impact of winglet rotation on the upper surface distribution also appears to have the most dominant influence at more midchord measurement stations rather than at either the leading or trailing edges of the main wing, with all midchord stations for most test conditions being substantially greater in magnitude than those close to the leading or trailing edges.

Comparing the winglet upper surface distributions from both Figs. 5 and 6, the somewhat ordered and uniform changes ($\Delta C_p \geq 0$ for Γ from 0 to -75 deg, and $\Delta C_p \leq 0$ for Γ from 0 to 7 deg) evident for all winglet deflection angles at $\alpha = 8$ deg all but disappear for $\alpha = 12$ deg. While under conditions of $\alpha = 8$ deg, the maximum change in ΔC_p for $\Gamma = 0$ to -75 deg ($\Delta C_p = 0.434$ at station 38) was found to be approximately three times that of ΔC_p for $\Gamma = 0$ to 75 deg ($\Delta C_p = -0.143$ at station 32), representing a substantial shift from the almost equal and opposite effect found for results on the baseline wing with winglet deflection either above and below the wing plane. Additionally, in a situation quite distinct from the influence of winglet rotation on the baseline wing element, the impact of winglet rotation on the winglet itself seems to bias toward the leading edge, particularly for $\Gamma < 0$ deg, which seems reasonable given the differences expected in aerodynamic loading, as the effective angle of attack of the winglet is changed from the baseline wing angle of attack initially ($\Gamma = 0$ deg) to $\alpha \approx 0$ deg at maximum winglet deflection magnitudes. For $\alpha = 12$ deg, a further increase of $\Delta\alpha = 4$ deg in angle of attack from $\alpha = 8$ deg leads to

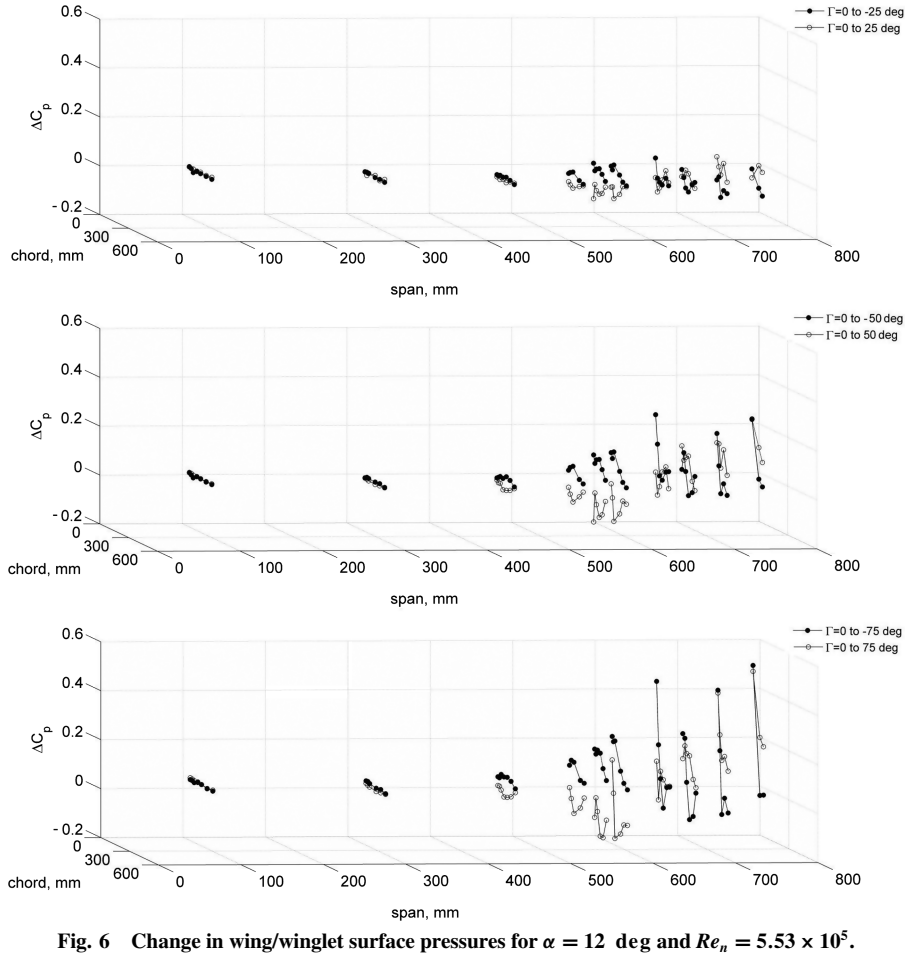

Fig. 6 Change in wing/winglet surface pressures for $\alpha = 12$ deg and $Re_n = 5.53 \times 10^5$.

a marked increased in disorder in winglet upper surface pressure, providing further evidence to the possibility that aerodynamic conditions are being encountered that are reducing winglet effectiveness at producing ultimate roll moment and/or promoting regions of flow separation.

IV. Conclusions

The use of articulated winglets on a baseline swept wing configuration to influence the surface pressure aerodynamics of a model flying wing has been experimentally investigated in this Note. From the surface pressure data taken from the upper wing and winglet surfaces, there is a substantial influence of winglet dihedral position on the main wing surface pressure. The ability of this concept to adjust and tailor this aerodynamic loading toward the main wing tip area may provide useful application to second-order performance and efficiency enhancements such as gust load alleviation.

Acknowledgment

This work has been supported by a Marie-Curie Excellence Research grant MEXT-CT-2003-002690 funded by the European Commission.

References

[1] McRuer, D., and Graham, D., "Flight Control Century: Triumphs of the Systems Approach," *Journal of Guidance, Control, and Dynamics*, Vol. 27, No. 2, 2004, pp. 161–173.
doi:10.2514/1.4586

[2] Jha, A. K., and Kudvasmart, J. N., "Morphing Aircraft Concepts, Classifications, and Challenges," *Proceedings of SPIE: Smart Structures and Materials 2004: Industrial and Commercial Applications of Smart Structures Technologies*, Vol. 5388, 2004, pp. 213–224.
doi:10.1117/12.544212

[3] Sanders, B., Eastep, F. E., and Forster, E., "Aerodynamic and Aeroelastic Characteristics of Wings with Conformal Control Surfaces for Morphing Aircraft," *Journal of Aircraft*, Vol. 40, No. 1, 2003, pp. 94–99.
doi:10.2514/2.3062

[4] Hall, J. M., "Executive Summary AFTI/F-111 Mission Adaptive Wing," Wright Research and Development Center TR 89-2083, Wright-Patterson AFB, OH, 1989.

[5] Knot, N. S., Zweber, J. V., Veley, D. E., Oz, H., and Eastep, F. E., "Flexible Composite Wing with Internal Actuation for Roll Maneuver," *Journal of Aircraft*, Vol. 39, No. 4, 2002, pp. 521–527.
doi:10.2514/2.2971

[6] Johnston, C. O., Mason, W. H., Han, C., and Inman, D. J., "Actuator-Work Concepts Applied to Unconventional Aerodynamic Control Devices," *Journal of Aircraft*, Vol. 44, No. 5, 2007, pp. 1459–1468.
doi:10.2514/1.26423

[7] Stanewsky, E., "Aerodynamic Benefits of Adaptive Wing Technology," *Aerospace Science and Technology*, Vol. 4, No. 7, 2000, pp. 439–452.
doi:10.1016/S1270-9638(00)01069-5

[8] Stanewsky, E., "Adaptive Wing and Flow Control Technology," *Progress in Aerospace Sciences*, Vol. 37, No. 7, 2001, pp. 583–667.
doi:10.1016/S0376-0421(01)00017-3

[9] Schultz, M. R., and Hyer, M. W., "A Morphing Concept Based on Unsymmetric Composite Laminates and Piezoceramic MFC Actuators," 45th AIAA/ASME/ASCE/AHS/ASC Structures, Structural Dynamics and Materials Conference, AIAA Paper 2004-1806, April 2004.

[10] Bourdin, P., Gatto, A., and Friswell, M. I., "Aircraft Control via Variable Cant-Angle Winglets," *Journal of Aircraft*, Vol. 45, No. 2, 2008, pp. 414–423.
doi:10.2514/1.27720